

# Enhanced TEC Maps Based on Different Space-Geodetic Observations

Jiantong Zhang, Michael Schmidt, Denise Dettmering,  
Liqiu Meng, Yueqin Zhu and Yanbin Wang

**Abstract** The ionosphere is defined as part of the upper earth's atmosphere, where the density of free electrons and ions is high enough to influence the propagation of electromagnetic radio frequency waves. The ionisation process is primarily depending on the Sun's activity and varies strongly with time, as well as with geographical location. The knowledge of the electron density is the critical point for many applications in positioning and navigation. During the last decade, dual-frequency Global Navigation Satellite Systems (GNSS), in particular the Global Positioning System (GPS) have become a promising tool for monitoring the Total Electron Content (TEC), i.e. the integral of the electron density along the ray-path between the transmitting satellite and the receiver. Hence, geometry-free GNSS measurements provide information on the electron density, which depends on spatial position and time, i.e. four-dimensional (4-D). At present the International GNSS Service (IGS) provides time-dependent vertical TEC (VTEC) maps based on more than 100 permanent ground stations; however, these stations are mainly located on the continents and provide less accurate results over the oceans. New space-based observation techniques, especially various Low-Earth-Orbiting (LEO) satellite missions such as *FORMOSAT-3/COSMIC* and *CHAMP*, as well as dual-frequency radar altimetry missions such as *Jason-1*, *Jason-2* and *Envisat*, can also contribute ionospheric evaluation on a global scale. The former get the TEC values from GPS-LEO occultation observations, whereas the latter provide VTEC observations from the on-board double-frequency radar altimeter. In order to enhance the IGS VTEC maps, i.e. balancing the insufficient GNSS coverage

---

J. Zhang (✉) · L. Meng · Y. Zhu  
Department of Cartography, Technische Universität München, Munich, Germany  
e-mail: jt.zhang@bv.tum.de

M. Schmidt · D. Dettmering  
Deutsches Geodätisches Forschungsinstitut (DGFI), Munich, Germany

Y. Zhu · Y. Wang  
China University of Mining and Technology, Beijing, China

over the sea, efficient and inexpensive occultation observations and altimetry measurements can be collected and utilized. In this way the IGS VTEC products can benefit from additional data sources. In this paper, we combine both occultation and altimetry measurements to enhance the IGS VTEC maps. Our model consists of a given reference part (background model) computed from the IGS VTEC products, and also of an unknown correction term. In contrary to the traditional spherical harmonic approach, we use a global multi-dimensional B-spline approach for modelling the unknown correction term. We rely on normalized endpoint-interpolating B-splines for modelling the latitude- and the time-dependency and trigonometric B-splines for the dependency on the longitude. Several constraints, e.g. for the poles, for meridian, have to be considered carefully. Since B-splines are localizing functions, i.e. they are characterized by a compact support, data gaps can be handled appropriately. The unknown series coefficients of our multi-dimensional B-spline expansion are calculable from the LEO and the altimetry measurements applying parameter estimation. The relative weighting between the different data sources, the prior information, and the constraints will be performed by Variance Component Estimation (VCE). We compare the enhanced VTEC maps between the combined approach, which is based on VCE, and a second approach using *FORMOSAT-3/COSMIC* and *Jason-1* data only within selected periods. It will be shown that an improvement from the additional data sources is visible in the areas with good data coverage. In regions with limited amount of observations the background model values from IGS will be conserved.

## 1 Introduction

The knowledge of electron density is the critical point in correcting electromagnetic measurements for ionospheric disturbances. Dual-frequency Global Navigation Satellite Systems (GNSS) and other observation techniques can be used to determine the Slant Total Electron Content (STEC) or the VTEC, i.e. TEC along the vertical. Many approaches can be used to produce ionosphere maps from data of the permanent GPS ground stations. IGS, for example, has more than 100 permanent GPS stations, and it provides global TEC map with a temporal of 2 h (Hernández-Pajares et al. 1999). However, the distribution of the IGS stations is rather heterogeneous, only few stations are located in the oceanic regions; but also on some continents such as Africa the GPS network is rather coarse-meshed. The space-borne GPS receivers flying on Low-Earth-Orbiting (LEO) satellites, such as the *FORMOSAT-3/COSMIC* satellites, *CHAMP* and *GRACE*, provide additional measurements for calculating VTEC maps on a global scale. Moreover, altimetry measurements, e.g. from *Jason-1*, *Jason-2* and *Envisat* also provide information for the VTEC maps, especially over the oceans. To combine both data sources on the basis of existing IGS VTEC maps, the enhanced VTEC map benefits from all data sources.

In our approach we decompose the VTEC model into two parts, namely (1) a global background model part, which is from the IGS VTEC products and (2) a correction part. The latter is modelled as a series expansion in terms of

localizing base functions. The occultation and altimetry measurements are utilized to calculate the unknown series coefficients by applying parameter estimation procedures.

In this contribution, we choose a multi-dimensional B-splines approach for modelling VTEC. To be more specific, we use so-called endpoint-interpolating quadratic B-splines for representing the data along latitude and time, as well as trigonometric B-splines along the longitude. We apply our method to *FORMO-SAT-3/COSMIC* and *Jason-1* measurements and obtain enhanced VTEC maps from the IGS VTEC maps. Due to the localisation feature of the B-spline base functions the combined model can handle data gaps appropriately (Schmidt et al. 2011); furthermore the evaluations show the advantages of a multi sensor analysis.

## 2 Related Work and Fundamentals

### 2.1 Related Work

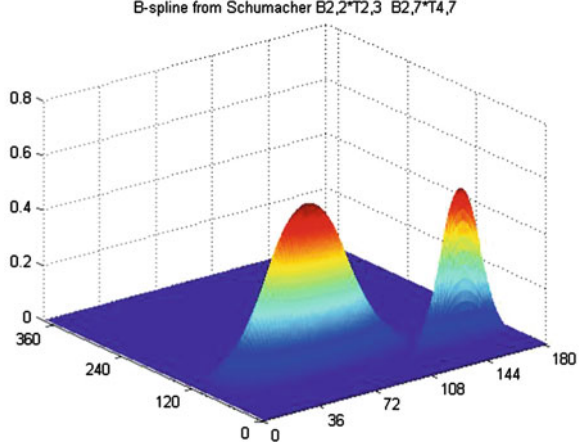
The IGS Ionosphere Working Group started to develop global ionospheric TEC products in 1998. It delivers global VTEC maps from different research groups with a temporal spacing of 2 h or less. Todorova et al. (2008) combined GNSS and altimetry data to produce VTEC maps. The approach is based on a spherical harmonic expansion and shows the potential for increasing the accuracy of TEC maps with manually setting weights for both data sources.

Spherical harmonic models can be appropriately used for global VTEC maps. For regional applications or in case of data gaps, localizing base functions are more qualified. Jekeli (2005) gives a review on different types of splines and their applications. Schmidt (2007) presented a B-spline approach to estimate the electron density regionally from GNSS observations; herein the International Reference Ionosphere (IRI) was used as background model; Zeilhofer et al. (2009) extended this approach to the 4-D case. Furthermore, Dettmering et al. (2011) introduced the combination of different space-geodetic observation techniques for regional ionosphere modelling. Schmidt et al. (2011) introduced trigonometric B-splines for global VTEC modeling and showed its advantages for unevenly distributed input data for simulated data sets. Here we use this approach on real data for estimating the VTEC model coefficients from different space-geodetic observation techniques.

### 2.2 Related Fundamentals

Schumaker and Traas (1991) developed spherical splines by combining so-called endpoint interpolating polynomial B-splines with trigonometric B-splines. Both

**Fig. 1** Products of B-splines  
 $N_{2,2}^2 \times T_{2,3}^3$  and  $N_{2,7}^2 \times T_{4,7}^3$



types of B-splines are compactly supported, i.e. the values are different from zero only in a finite range within the specific interval  $I = [V_{\min}, V_{\max}]$ . The normalized quadratic endpoint interpolating B-splines of order  $m$  are defined recursively at a sequence of non-decreasing knots  $t_0^j, t_1^j, \dots, t_{m_j+2}^j$  with  $k = 0, \dots, m_j - 1$  and  $m = 1, \dots, d$ , with  $m_j = 2^j + m$  as shown in the Eqs. (1) and (2):

$$N_{j,k}^m(x) = \frac{x - t_k^j}{t_{k+m}^j - t_k^j} N_{j,k}^{m-1}(x) + \frac{t_{k+m+1}^j - x}{t_{k+m+1}^j - t_{k+1}^j} N_{j,k+1}^{m-1}(x) \quad (1)$$

with the initial values

$$N_{j,k}^0(x) = \begin{cases} 1 & \text{for } t_k^j \leq x < t_{k+1}^j \\ 0 & \text{else} \end{cases} \quad (2)$$

In case of global modelling by means of the spherical B-splines a globally defined function  $f$  is restricted to  $f(0, \varphi, t) = f(2\pi, \varphi, t)$ . Thus, the normalized periodic trigonometric B-splines can be used. These splines can be calculated via a recurrence relation. Suppose for the knots w.r.t. the longitude the inequalities  $\dots < \lambda_l^j < \lambda_{l+1}^j < \dots$  the definition equation of the trigonometric B-splines reads

$$T_{j,l}^m(\lambda) = \frac{\sin \frac{\lambda_l^j - \lambda_l^j}{2}}{\sin \frac{\lambda_{l+m-1}^j - \lambda_l^j}{2}} T_l^{m-1}(\lambda) + \frac{\sin \frac{\lambda_{l+m}^j - \lambda_l^j}{2}}{\sin \frac{\lambda_{l+m}^j - \lambda_{l+1}^j}{2}} T_{l+1}^{m-1}(\lambda) \quad (3)$$

with  $T_{j,l}^1(\lambda) = \begin{cases} 1, & \lambda_l \leq \lambda < \lambda_{l+1} \\ 0, & \text{otherwise} \end{cases}$ ,  $l = 0, \dots, L_j - 1$  with  $L_j = 3 \cdot 2^j$ ; the level value  $J$  defines the number of distinct knot points,  $m$  is the order of the splines.

Figure 1 visualizes the product of selected  $N_j^2$  and  $T_j^3$  base functions; these products are also known as tensor products. Note, the higher the level value  $J$  is

chosen the sharper is the peak and the finer are the structures which can be modelled.

The study which is introduced in the next section uses simplified gradations of positioning and orientation errors. More specifically, a distinction will only be made between erroneous and error-free positioning and/or orientation.

### 3 Global Enhanced VTEC Model

#### 3.1 Enhanced Global VTEC Approach for Single Data Source

In analogy to the enhanced model presented by Schmidt (2007), VTEC can be decomposed into the background model  $VTEC_{ref}(p, t)$  and a correction term  $\Delta VTEC(p, t)$  for the observation on location  $p$  at time  $t$

$$VTEC(p, t) = VTEC_{ref}(p, t) + \Delta VTEC(p, t) \quad (4)$$

Schmidt discussed different approaches to model the correction term  $\Delta VTEC(p, t)$  in Eq. (4) (Schmidt et al. 2007); with some modifications the model can be extended to a global approach (Schmidt et al. 2011). Here we assume that  $\Delta VTEC(p, t)$  is represented by the series expansion

$$\Delta VTEC(p, t) = \sum_{k_1=0}^{M_{J_1}-1} \sum_{k_2=0}^{M_{J_2}-1} \sum_{k_3=0}^{M_{J_3}-1} d_{k_1, k_2, k_3}^{J_1, J_2, J_3} \phi_{k_1}^{J_1}(\varphi) T_{k_2}^{J_2}(\lambda) \phi_{k_3}^{J_3}(t) \quad (5)$$

wherein  $p$  means the observation site with latitude  $\varphi$  and longitude  $\lambda$ ;  $t$  means the time;  $\phi_k^J(t) = N_{J,k}^2(t)$  are the normalized quadratic B-splines as defined in Eq. (1) with  $m = d = 2$ ,  $T_k^J(\lambda) = T_{J,k}^3(\lambda)$  the periodic trigonometric B-splines according to Eq. (3) with  $m = 3$ .

Considering the time dependency, we divide the observation period  $[t_s, t_e]$  into  $L$  subintervals  $\Delta t = \frac{t_e - t_s}{L}$ , i.e.  $L = 6$  in our test. The correction term  $\Delta VTEC$  is the difference between the background model and the real measurements considering the measurement error  $e$ . Under this assumption we establish the Gauss-Markov model from Eq. (5)

$$y + e = Ad \text{ with } D(y) = \sigma_y^2 P_y^{-1} \quad (6)$$

On the left side of Eq. (6) we introduce the  $n \times 1$  observation vector  $y = [y_1, y_2, \dots, y_n]'$  and the  $n \times 1$  vector  $e = [e_1, e_2, \dots, e_n]'$  of the measurement errors. Furthermore,  $d = [d_{0,0,0}^{J_1, J_2, J_3}, \dots, d_{m_{J_1}-1, m_{J_2}-1, m_{J_3}-1}^{J_1, J_2, J_3}]'$  means the  $u \times 1$  vector of the unknown scaling coefficients, whereas the  $n \times u$  coefficient matrix  $A$  collects the spatio-temporal tensor product B-spline functions

$$A = \begin{bmatrix} a_{0,0,0}^{J_1, J_2, J_3}(\varphi_1, \lambda_1, t_1) & \cdots & a_{m_{J_1}-1, m_{J_2}-1, m_{J_3}-1}^{J_1, J_2, J_3}(\varphi_1, \lambda_1, t_1) \\ \vdots & \ddots & \vdots \\ a_{0,0,0}^{J_1, J_2, J_3}(\varphi_n, \lambda_n, t_n) & \cdots & a_{m_{J_1}-1, m_{J_2}-1, m_{J_3}-1}^{J_1, J_2, J_3}(\varphi_n, \lambda_n, t_n) \end{bmatrix} \quad (7)$$

Herein  $a_{0,0,0}^{J_1, J_2, J_3}$  is the product of  $\phi_0^{J_1}(\varphi_1)T_0^{J_2}(\lambda_1)\phi_0^{J_3}(t_1)$ .

In order to evaluate the unknowns *d* additional constraints have to be considered (Schumaker and Traas 1991)

$$H \times d = w \quad (8)$$

whereas  $H$  and  $w$  means an  $r \times u$  given matrix and an  $[r \times 1]$  given vector of the constraints for Eq. (6) with  $u = I \cdot J \cdot K$  with  $I = m_{J_1-1}$ ;  $J = m_{J_2-1}$ ;  $K = m_{J_3-1}$ . Consequently, the number of constraints depends on the selected levels  $J_1$ ,  $J_2$  and  $J_3$  for the B-splines.

From Eqs. (6) and (8) a Gauss-Markov model with constraints is defined. Assuming the constraints in Eq (8) as an additional observation equation including a  $r \times 1$  error vector  $v$  this model can be rewritten as

$$\begin{cases} Ad = y + e \\ Hd = w + v \end{cases} \text{ with } D\left(\begin{bmatrix} y \\ w \end{bmatrix}\right) = \sigma^2 \begin{bmatrix} P^{-1} & 0 \\ 0 & cI \end{bmatrix} \quad (9)$$

wherein  $c$  with  $c > 0$  is the weight factor for constraints. With the  $r \times r$  unit matrix  $I$  we set equal weights for pseudo measurements  $0$ . The least squares estimator is given by Koch (1999) and reads

$$\hat{d} = (A'PA + H'H/c)^{-1}(A'Py + H'w/c) \quad (10)$$

So the correction term for a new given location and time can be estimated by estimator  $\hat{d}$  in Eq. (9):

$$y_{new} = \Delta \widehat{VTEC}(p_{new}, t_{new}) = (A_{new}) \cdot \hat{d} \quad (11)$$

### 3.2 Hypotheses Global VTEC Model Based on Multi Observation

Measurements from different platforms, i.e. different satellite missions, have their own characteristics and accuracy levels. Moreover, several studies have shown that altimetry such as the *Jason-1* mission overestimate VTEC by about 3-4 TECU compared to the values delivered by GNSS (Brunini et al. 2005). Considering different ionosphere measurements at the same time, a proper weighting scheme should be chosen in order to account for the accuracy level of each data source  $i$ , so the new observation equations for each measurement techniques reads

$$A_i \cdot d = y_i + e_i \text{ with } i \in \{1, \dots, m\} \quad (12)$$

with

$$D\left(\begin{bmatrix} y_1 \\ \vdots \\ y_i \\ \vdots \\ y_m \end{bmatrix}\right) = \begin{bmatrix} \sigma_1^2 P_1^{-1} & \cdots & 0 & \cdots & 0 \\ \vdots & \ddots & \vdots & \ddots & \vdots \\ 0 & \cdots & \sigma_i^2 P_i^{-1} & \cdots & 0 \\ \vdots & \cdots & \vdots & \ddots & \vdots \\ 0 & \cdots & 0 & \cdots & \sigma_m^2 P_m^{-1} \end{bmatrix}$$

here in,  $m$  indicates the number of different measurement types;  $A_i$  and  $d$  are the same as in Eq. (6),  $y_i$  is the observation vector for the  $i$ th type of measurement. The covariance factors  $\sigma_i^2$  are unknown parameters since the relative weighting  $P_i$  of different kinds of observations is usually unknown. The selection of weights for different type of measurements is the most important step for this model; however, it is difficult to choose the weights although Todorova et al. (2008) manually set the weights in order to generate the TEC map from multiple data sources and get positive results.

An alternative approach is to choose these different weights automatically, e.g. by VCE (Koch and Kusche 2002), it estimates the variance factors iteratively. Moreover, the ratio of these weights can be used as regularization parameters (Arsenin and Krianev 1992). In the framework of Bayesian inference prior information for the unknown parameters is introduced, in this way we may add a new type of observation equation supposing the expectation vector and the corresponding covariance matrix of the unknown coefficient vector are given according to

$$d = \mu + e_\mu \quad (13)$$

with

$$D(d|\sigma_\mu^2) = \sigma_\mu^2 \cdot P_\mu^{-1}$$

here in, the  $u \times 1$  vector  $\mu$  is the prior information on the unknown parameters, and  $P_\mu$  is the corresponding given  $u \times u$  weight matrix. In addition to the groups of measurements (*FORMOSAT-3/COSMIC*, *Jason-1*), the constraints are also treated as one observation group just like the prior information which are necessary to account for areas and epochs without measurements, furthermore, it assumes the constraint has also error vector  $v$ . So the extended Gauss-Markov model is

$$\begin{bmatrix} A_1 \\ A_2 \\ H \\ I \end{bmatrix} \cdot d = \begin{bmatrix} y_1 \\ y_2 \\ w \\ \mu \end{bmatrix} + \begin{bmatrix} e_1 \\ e_2 \\ v \\ e_\mu \end{bmatrix} \quad (14)$$

with

$$D \left( \begin{bmatrix} y_1 \\ y_2 \\ w \\ \mu \end{bmatrix} \right) = \begin{bmatrix} \sigma_1^2 P_1^{-1} & 0 & 0 & 0 \\ 0 & \sigma_2^2 P_2^{-1} & 0 & 0 \\ 0 & 0 & \sigma_w^2 P_w^{-1} & 0 \\ 0 & 0 & 0 & \sigma_\mu^2 P_\mu^{-1} \end{bmatrix}$$

herein,  $H$  and  $w$  are already defined in Eq. (9);  $A_1$  and  $A_2$  are related to the *FORMOSAT-3/COSMIC* data and the altimetry *Jason-1* observations, respectively. Note that we set  $m = 2$ , since we just have *FORMOSAT-3/COSMIC* and *Jason-1* in our test. Then, the estimation  $\hat{d}$  of the unknown parameter vector  $d$  follows from the normal equations:

$$\begin{aligned} & \left( \frac{1}{\sigma_1^2} A_1' P_1 A_1 + \frac{1}{\sigma_2^2} A_2' P_2 A_2 + \frac{1}{\sigma_w^2} A_w' P_w A_w + \frac{1}{\sigma_\mu^2} P_\mu \right) \hat{d} \\ &= \frac{1}{\sigma_1^2} A_1' P_1 y_1 + \frac{1}{\sigma_2^2} A_2' P_2 y_2 + \frac{1}{\sigma_w^2} A_w' P_w y_w + \frac{1}{\sigma_\mu^2} P_\mu \mu \end{aligned} \quad (15)$$

The variance  $\sigma_i^2$  can be estimated iteratively using different strategies, refer to Koch and Kusche (2002) for more detail. Analogously to Eq. (12), the reconstruction of  $\widehat{\Delta VTEC}$  can be estimated by the estimator  $\hat{d}$  from Eq. (15) for any point  $p$  within the observation period  $[t_s, t_e]$ .

## 4 Numerical Comparisons

### 4.1 Data Sets

In our investigation, we choose the measurements from *FORMOSAT-3/COSMIC* and *Jason-1* as our test data sets. The occultation measurements have a homogeneous distribution over the sphere comparing to the altimetry observations. We choose 1 day with maximum number of measurements as test data set in order to reach a high model resolution which requires enough observations to estimate the unknown parameters, i.e. the B-spline coefficients of high level  $J$ . Figure 2 shows the input measurements on July 24th, 2006.

To get the input difference data between the measurements and the background model  $\widehat{\Delta VTEC}$  has been calculated for both observation types w.r.t. IGS VTEC. Figure 3 shows these differences for 24 h: the mean value for the difference from *FORMOSAT-3/COSMIC* is around  $-2.53$  TECU; on the contrary, the corresponding value for *Jason-1* is  $+2.55$  TECU.



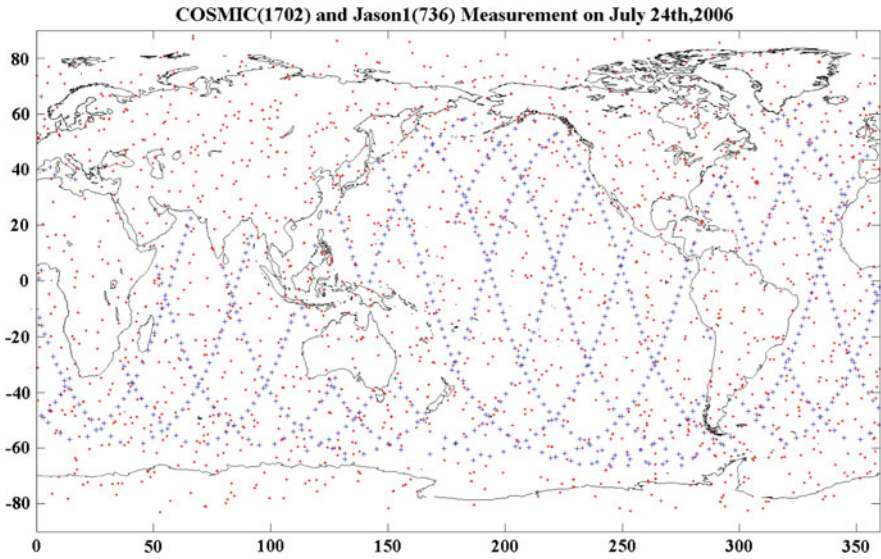


Fig. 2 Distribution of *FORMOSAT-3/COSMIC* and *Jason-1* measurements

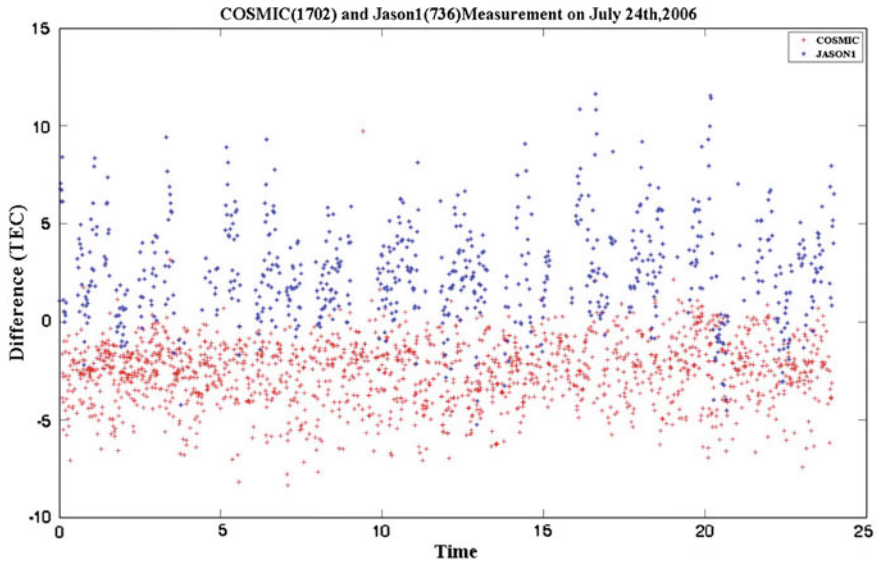


Fig. 3 VTEC differences between two types of measurements comparing to IGS model

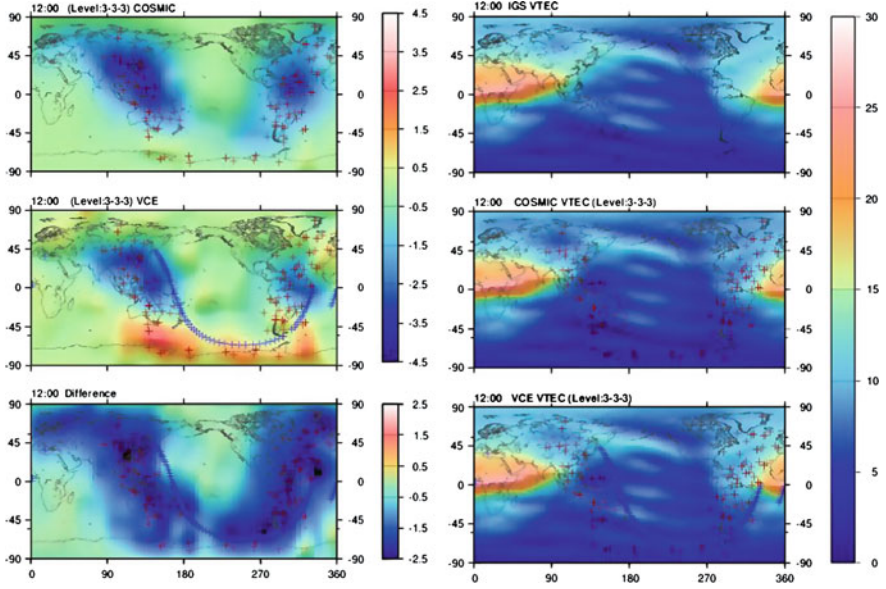


Fig. 4 VTEC corrections (left side) and reconstructions (right side) from both approaches

## 4.2 Results and Discussion

We compute the correction term as well as the reconstructed VTEC maps by Eqs. (13) and (5) respectively. In this test, we set  $J_1 = 3$ ,  $J_2 = 3$  and  $J_3 = 3$  for Eq. (5), let  $K_1 = M_{J_1} - 1$ ,  $K_2 = M_{J_2} - 1$ ,  $K_3 = M_{J_3} - 1$  i.e. it has  $K_1 = 24$ ,  $K_2 = 10$ ,  $K_3 = 10$  local functions for longitude, latitude and time respectively; thus we have 2,400 unknowns. In order to estimate the bias of both data sources, two more unknowns are added, that means the model has 2,402 unknowns.

The correction value at a specific time depends on the location and VTEC intensity of the input measurements. Figure 4 (a–f) shows the map of the correction terms from each approach at 12:00 UT. First row left (4a), COSMIC corrections only; first row right (4d), IGS VTEC; second row left (4b), VCE approach; second row right (4e), IGS + COSMIC corrections; last row left (4c), differences between COSMIC and VCE solution; last row right (4f), IGS + VCE corrections. The unit is in TECU, and the COSMIC data is indicated with red '+', whereas the *Jason-1* data is indicated with blue '+'. Obviously, the result of the combined approach in Fig. 4b shows the modifications w.r.t the *FORMOSAT-3/COSMIC* approach, especially in the areas with altimetry measurements.

The difference of the correction term from both approaches has been calculated using Eq. (16), revealing values between (−2.5 and 0.5) TECU, see Fig. 4c:

$$\Delta d = \Delta \widehat{VTEC}_{\text{cosmic}} - \Delta \widehat{VTEC}_{\text{VCE}} \quad (16)$$

**Table 1** Standard deviations and offsets in the test

	<i>FORMOSAT-3/COSMIC</i>		<i>Jason-1</i>		Constraints	Prior information
	Input	Result	Input	Result		
$\sigma_i$	1.67	0.82	2.55	1.95	0.04	1.88
$\lambda_i$	1		0.18		420.25	0.19
Bias	-2.18		2.71		-	-

To reconstruct the VTEC maps, we choose a regular grid with  $\Delta\lambda = 5^\circ$ ,  $\Delta\varphi = 2.5^\circ$  and  $\Delta t = 2$  h.

The proposed integrated global model in Eq. (14) has the ability to revise the background model in Eq. (4). No matter with only one data source (Fig. 4a) or with two data sources (Fig. 4b), it generates the modifications from the real measurements, and it shows less influence from the data gaps, i.e. the area without input data. The result in Fig. 4b presents the benefit from altimetry data especially along the satellite ground track. The difference between two approaches in Fig. 4c also shows that most modifications are located along the orbit.

In the VCE approach, the variance has been estimated iteratively till its convergence. Table 1 shows the computed variances and biases. The variance of the constraints is the smallest because the constraint as observation is assumed to be ideal measurements which have better precision than the real measurements from *FORMOSAT-3/COSMIC* and *Jason-1* in Eq. (14). As shown in Table 1, *FORMOSAT-3/COSMIC* has more stable measurements than *Jason-1*, and the bias from the estimated results is also correct comparing to the mean value in the test data sets. The standard deviation of *FORMOSAT-3/COSMIC* decreases from 1.67 to 0.82, whereas the standard deviation of *Jason-1* drops from 2.55 to 1.95, so this also verifies the efficient combination of both data sources, as shown in Table 1. In order to estimate the relative weighting of different data source, we rearrange the Eq. (15) by multiplying  $\sigma_1^2$  on both side

$$\begin{aligned}
 &(\lambda_1 A'_1 P_1 A_1 + \lambda_2 A'_2 P_2 A_2 + \lambda_3 A'_w P_w A_w + \lambda_4 P_\mu) \hat{d} \\
 &= \lambda_1 A'_1 P_1 y_1 + \lambda_2 A'_2 P_2 y_2 + \lambda_3 A'_w P_w y_w + \lambda_4 P_\mu \mu
 \end{aligned} \tag{17}$$

with the regularization parameters  $\lambda_1 = 1$ ;  $\lambda_2 = \frac{\sigma_1^2}{\sigma_2^2}$ ;  $\lambda_3 = \frac{\sigma_1^2}{\sigma_w^2}$ ;  $\lambda_4 = \frac{\sigma_1^2}{\sigma_\mu^2}$ .

In Table 1, comparing to *FORMOSAT-3/COSMIC*, *Jason-1* has lower influence because the distribution is limited by its ground track, which has unbalanced temporal distribution. The prior information  $I$  in Eq. (14) has also small influence in the computation, which indicates that the prior knowledge is not the decisive factor in this model. Comparing to the real measurements and prior information, the constraint  $H$  in Eq. (14) has strong influence in the model, because it has the ability to make sure that the results fulfill all constraints in Eq. (8).

The standard deviation  $\sigma_i$  is according to the Eq. (18), which can be calculated by:

$$\sigma_i = \sqrt{\frac{\hat{e}_i P_i \hat{e}_i}{r_i}} \tag{18}$$

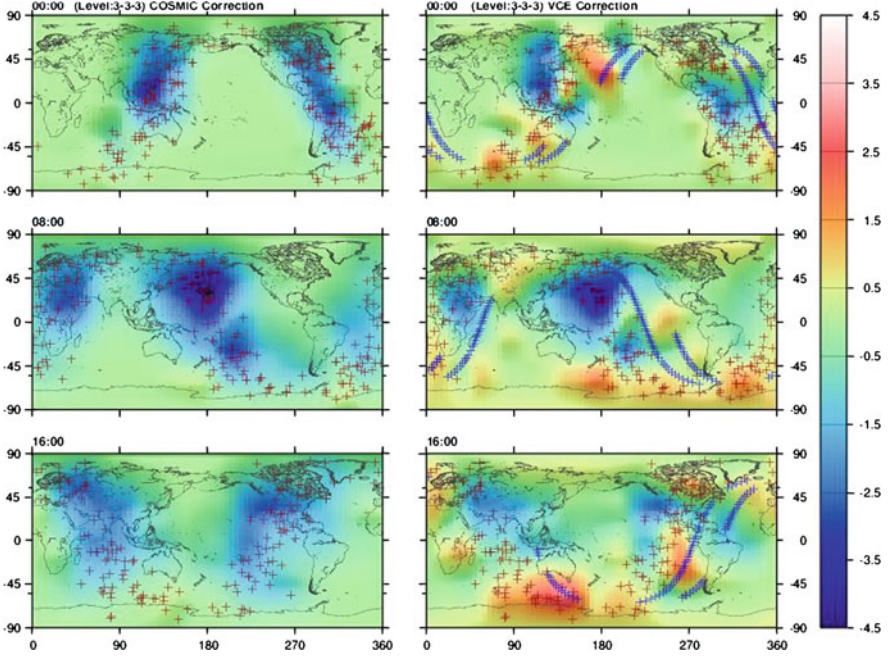


**Fig. 5** Corrections term for both approaches (in TECU)

with  $\hat{e}_i = \hat{y}_i - y_i$ ;  $P_i$  is the same as in Eq. (14),  $r_i$  is the partial redundancies, Koch and Kusche (2002) calculated the redundancy

$$r_i = n_i - \text{tr}\left(\frac{1}{\sigma_i^2} A_i' P_i A_i N^{-1}\right) \quad (19)$$

and

$$r_\mu = n_\mu - \text{tr}\left(\frac{1}{\sigma_\mu^2} P_\mu N^{-1}\right)$$

for different observation types  $i$  and prior information respectively.

The enhanced VTEC maps can be reconstructed for a given position and time within the observation period. Figure 5 only shows part of the reconstructed VTEC maps at 8 h interval from both approaches, whereas Fig. 6 shows the enhanced VTEC maps in the same epoch as Fig. 5.

Usually the proposed model with a higher resolution provides better approximation of the VTEC maps. However, it requires more measurements to estimate the unknown parameters, for instance, if it choose  $J_1 = 3$ ,  $J_2 = 4$ ,  $J_3 = 3$  in Eq. (5) respectively, i.e.  $K_1 = 24$ ,  $K_2 = 18$ ,  $K_3 = 10$ , that means it has 4,320 unknowns. Whereas it needs 17,280 unknowns if it selects  $J_1 = 4$ ,  $J_2 = 5$ ,  $J_3 = 3$ , so it is reasonable in near future if more data sources if new satellite missions can provide such amount of data with homogeneous global distribution.

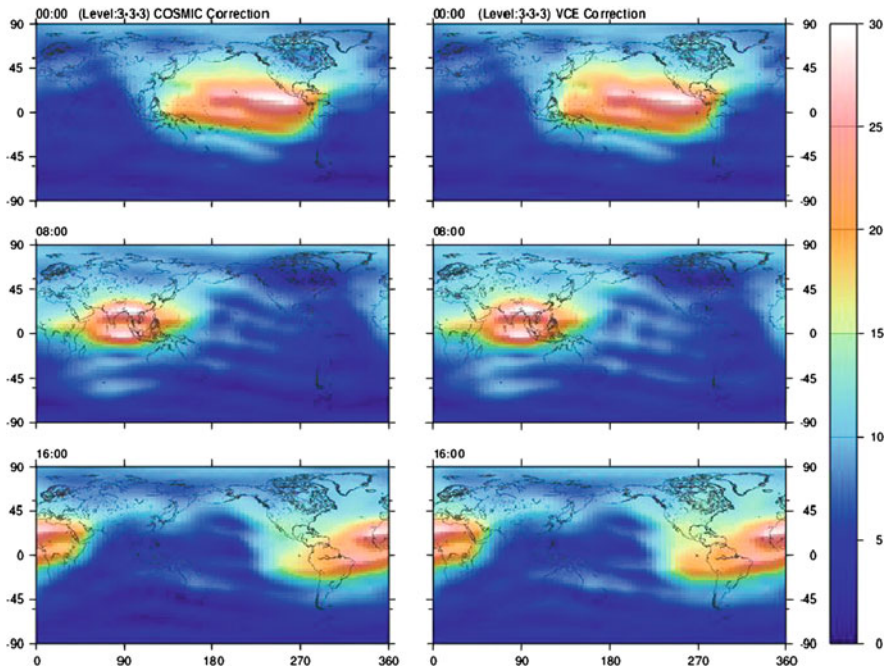


Fig. 6 Enhanced VTEC maps based on IGS VTEC (in TECU)

## 5 Conclusion

In this paper, we present an efficient fusion approach for combining two different data sources to generate enhanced VTEC maps by global B-splines model; moreover, using more than two different data sources is also possible in our approach. The model is separated into a background part (IGS VTEC map) and a correction part whose unknown coefficients are estimated based on measurements from LEO osculations and altimetry.

In the numerical test, we use the *FORMOSAT-3/COSMIC* as well as *Jason-1* observations for one selected day to test the approach. For the combination of both data types, variance component estimation is applied. Both data types show systematic offsets of about 2 TECU with respect to GPS (with different sign). The *FORMOSAT-3/COSMIC* data in our test has stronger regularization ability than *Jason-1*. The enhanced VTEC maps show an enhancement about  $\pm 3$  TECU. In the maps showing the deviation (Fig. 4b) i.e. the enhancement about the additional data source can be clearly seen.

The results in this paper are only based on one specific day. To get a more robust assessment, a longer time period is necessary in order to check the influence of different ionospheric conditions and different data coverage through more/other measurements. Although the enhancement is obviously in the correction map, additional validation procedures are necessary, for instance, the cross-validation or validation from other independent data source, and it's our future work.



## References

- Arsenin VY, Krianev AV (1992) Generalized maximum likelihood method and its application for solving ill-posed problems. In: Tikhonov A (ed) Ill-posed problems in natural sciences. TVP Science Publishers, Moscow, pp 3–12
- Brunini C, Meza A, Bosch W (2005) Temporal and spatial variability of the bias between TOPEX- and GPS-derived total electron content. *J Geodesy* 79:175–188
- Dettmering D, Schmidt M, Heinkelmann R, Seitz M (2011) Combination of different space-geodetic observations for regional ionosphere modeling. *J Geodesy* 85(12):989–998. DOI:[10.1007/s00190-010-0423-1](https://doi.org/10.1007/s00190-010-0423-1)
- Hernández-Pajares M, Juan JM, Sanz J, Orus R, Garcia-Rigo A, Feltens J, Komjathy A, Schaer SC, Krankowski A (1999) The IGS VTEC map: a reliable source of ionospheric information since 1998. *J Geodesy* 83:263–275
- Jekeli C (2005) Spline representations of functions on a sphere for geopotential modeling. Technical report no. 475, Ohio state university, Ohio
- Koch KR (1999) Parameter estimation and hypothesis testing in linear models. Springer, Berlin
- Koch KR, Kusche J (2002) Regularization of geopotential determination from satellite data by variance components. *J Geodesy* 76:259–268. doi:[10.1007/s00190-002-0245-x](https://doi.org/10.1007/s00190-002-0245-x)
- Schmidt M (2007) Wavelet modelling in support of IRI. *Adv Space Res* 39(5):932–940
- Schmidt M, Bilitza D, Shum CK, Zeilhofer C (2007) Regional 4-D modelling of the ionospheric electron content. *Adv Space Res* 42:782–790
- Schmidt M, Dettmering D, Mößmer M, Wang Y, Zhang J (2011) Comparison of spherical harmonic and B-spline model for VTEC. *Radio Sci* 46:RS0D11. doi:[10.1029/2010RS004609](https://doi.org/10.1029/2010RS004609)
- Schumaker LL, Traas C (1991) Fitting scattered data on sphere like surface using tensor products of trigonometric and polynomial splines. *Numerische Mathematik* 60(1):133–144. DOI:[10.1007/BF01385718](https://doi.org/10.1007/BF01385718)
- Todorova S, Hobiger T, Schuh H (2008) Using the global navigation satellite system and satellite altimetry for combined global ionosphere maps. *Adv Space Res* 42(4):727–736
- Zeilhofer C, Schmidt M, Bilitza D, Shum CK (2009) Regional 4-D modelling of the ionospheric electron density from satellite data and IRI. *Adv Space Res* 43:1669–1675

Earth Observation of Global Changes (EOGC)

Krisp, J.M.; Meng, L.; Pail, R.; Stilla, U. (Eds.)

2013, XXIV, 293 p., Hardcover

ISBN: 978-3-642-32713-1